

# NON-LINEAR EDDY VISCOSITY TURBULENCE MODELING IN HYDRA-TH FOR FUEL RELATED APPLICATIONS

**Ben Magolan, Emilio Baglietto**

Department of Nuclear Science and Engineering  
Massachusetts Institute of Technology  
77 Massachusetts Avenue, 24-107, Cambridge, MA 02139  
bmagolan@mit.edu; emiliob@mit.edu

**Mark Christon**

Los Alamos National Laboratory  
P.O. Box 1663, Los Alamos, NM 87545  
christon@lanl.gov

**Thomas Smith**

Sandia National Laboratories  
P.O. Box 5800, Albuquerque, NM 87185  
tmsmith@sandia.gov

## ABSTRACT

A quadratic  $k$ - $\varepsilon$  eddy viscosity turbulence model has been implemented in Hydra-TH, a Computational Fluid Dynamics (CFD) software being developed at Los Alamos National Laboratory, to support the thermal-hydraulics modeling needs of the CASL program. This model adopts a non-linear extension of the stress-strain relationship that allows it to capture the anisotropy of flow conditions. Modeling this behavior is essential for accurate simulation and prediction of the flow profile in fuel rod arrays, where secondary flow vortices arise and act to modify the flow profile. The model formulation and implementation in Hydra-TH is briefly discussed, followed by a validation of test cases for triangular and square rod fuel arrays.

## KEYWORDS

Turbulence,  $k$ - $\varepsilon$ , NLEVM, Hydra-TH

## 1. INTRODUCTION

Detailed prediction of the flow distribution inside fuel assemblies is essential for the design and safe operation of nuclear systems. Since the flow distribution cannot be calculated with exact analytical methods, numerical modeling and CFD simulation are needed to characterize this behavior. The high Reynolds number flows characteristic of nuclear reactor fuel assemblies preclude the use of Direct Numerical Simulation (DNS) and Large Eddy Simulation (LES) for full assembly and core calculations. Practical engineering CFD simulations must therefore be based on the Reynolds-Averaged Navier-Stokes (RANS) equations with appropriate turbulence modeling. It is therefore of paramount interest to design and implement RANS turbulence models that are capable of resolving these complex flow structures.

The coolant flow distribution in a fuel assembly is a highly complex, anisotropic phenomenon. The complicated flow structure and turbulence redistribution has been observed in numerous fuel bundle

experiments (e.g. Trupp and Azad [1]; Carajilescov and Todreas [2]; Rehme [3]). Anisotropy in the near-wall region leads to the formation of a secondary flow that spirals through the bundle. The secondary motion acts to redistribute the flow structure and smooth out wall shear stress and axial velocity profiles. Such flows—termed secondary flow of Prandtl 2<sup>nd</sup> kind—were originally postulated by Nikuradse [4] in 1926, but eluded experimental measurement until 1988 when Vonka [5] demonstrated that such flows are approximately 0.1% that of the primary velocity by using laser Doppler velocimetry.

A myriad of two-equation RANS turbulence models have been developed (e.g.  $k$ - $\epsilon$ ,  $k$ - $\omega$ , SST). Such models are predicated on the Boussinesq hypothesis, which assumes the turbulent stresses are proportional to the mean velocity gradients of the flow. This approximation assumes that the eddy viscosity is isotropic, and is therefore incapable of capturing the anisotropy of the Reynolds stresses. Reynolds Stress Models (RSM) can be used to model the flow anisotropy. However, the challenges in modeling the higher order closure terms based on general validity physical arguments still strongly limits their robustness

Non-linear eddy viscosity models (NLEVM) are an extension of standard two-equation turbulence models, whereby a non-linear stress-strain relationship is applied. The concept of NLEVMs originated from Lumley [6] and Pope [7], who demonstrated that a generalized non-linear stress-strain relationship was mathematically equivalent to an explicit algebraic Reynolds stress model (EARSM). The most commonly adopted formulation for NLEVMs is cubic in nature, with the cubic terms being sufficient to include sensitivity to streamline curvature and rotation. The quadratic terms capture the normal stress anisotropy and have been demonstrated to be sufficient for fuel related applications [8] [9].

A quadratic formulation of the NLEVM has therefore been implemented in Hydra-TH in order to enhance the simulation capability of reactor systems and support the goals of the CASL program. Implementation of this quadratic model necessitated the restructuring of the code architecture—in particular, the  $k$ - $\epsilon$  class structure and inheritance schemes—and an explicit treatment of the quadratic stress terms in the momentum equation. The model implementation has been validated through simulation of test cases for triangular and square rod fuel arrays. A rigorous sensitivity study of the triangular array has also been performed to determine best practices and guidelines for the model’s application to fuel related problems.

## 2. MODEL DESCRIPTION

All NLEVMs are founded on the same basic stress-strain relationship, differing with respect to formulation of model coefficients. The quadratic form of the NLEVM developed by Baglietto and Ninokata [10] was selected for implementation in Hydra-TH. This formulation respects the constraints of realizability, which mandate that the turbulent normal stresses must remain positive and Schwarz’ inequality must be satisfied between fluctuating quantities. Satisfaction of these constraints leads to coefficients that are not constant, but rather vary with the mean flow deformation rate.

### 2.1. Model Formulation

The turbulent kinetic energy  $k$  and turbulent dissipation rate  $\epsilon$  transport equations are defined as follows:

$$\frac{\partial}{\partial t}(\rho k) + \frac{\partial(\rho u_j k)}{\partial x_j} = \frac{\partial}{\partial x_j} \left[ \left( \mu + \frac{\mu_t}{\sigma_k} \right) \frac{\partial k}{\partial x_j} \right] + P_k - \rho \epsilon \quad (1)$$

$$\frac{\partial}{\partial t}(\rho \epsilon) + \frac{\partial(\rho u_j \epsilon)}{\partial x_j} = \frac{\partial}{\partial x_j} \left[ \left( \mu + \frac{\mu_t}{\sigma_\epsilon} \right) \frac{\partial \epsilon}{\partial x_j} \right] + C_{\epsilon 1} \frac{\epsilon}{k} P_k - C_{\epsilon 2} \rho \frac{\epsilon^2}{k} \quad (2)$$

where the production term  $P_k$  and turbulent viscosity  $\mu_t$  are

$$P_k = -\overline{\rho u'_i u'_j} \frac{\partial u_i}{\partial x_j} \quad (3)$$

$$\mu_t = C_\mu \frac{\rho k^2}{\epsilon} \quad (4)$$

The empirical coefficients arising in Eqs. (1) and (2) derive from the work of Launder and Spalding [11], who championed the standard  $k$ - $\epsilon$  model, and are summarized in Table I for completeness. The realizability of the model is enforced by the  $C_\mu$  coefficient, which is no longer a constant as in the original formulation, but rather is expressed as a function of the mean shear invariant  $S$ :

$$C_\mu = \frac{2/3}{3.9 + S} \quad (5)$$

$$S = \frac{k}{\epsilon} \sqrt{2S_{ij}S_{ij}} \quad (6)$$

$$S_{ij} = \frac{1}{2} \left( \frac{\partial u_i}{\partial x_j} + \frac{\partial u_j}{\partial x_i} \right) \quad (7)$$

The Reynolds stress tensor is defined by the following expression:

$$\begin{aligned} \overline{\rho u'_i u'_j} = & \frac{2}{3} \rho k \delta_{ij} - 2\mu_t S_{ij} \\ & + 4\mu_t \frac{k}{\epsilon} \left\{ C_1 \left[ S_{ik}S_{kj} - \frac{1}{3} \delta_{ij}S_{kl}S_{kl} \right] + C_2 \left[ \Omega_{ik}S_{kj} + \Omega_{jk}S_{ki} \right] + C_3 \left[ \Omega_{ik}\Omega_{jk} - \frac{1}{3} \delta_{ij}\Omega_{kl}\Omega_{kl} \right] \right\} \end{aligned} \quad (8)$$

where the mean rotation rate tensor  $\Omega_{ij}$  is

$$\Omega_{ij} = \frac{1}{2} \left( \frac{\partial u_i}{\partial x_j} - \frac{\partial u_j}{\partial x_i} \right) \quad (9)$$

The first line of Eq. (8) represents the linear formulation of the Reynolds stresses that is adopted in isotropic eddy viscosity models such as the standard  $k$ - $\epsilon$  model. The second line denotes the quadratic stress terms that serve to provide a more complete description of the anisotropy of the normal stresses. The coefficients  $C_1$ - $C_3$  are not model constants, but instead vary with the mean flow deformation rate:

$$C_1 = \frac{C_{NL1}}{(C_{NL4} + C_{NL5}S^3)C_\mu} \quad (10)$$

$$C_2 = \frac{C_{NL2}}{(C_{NL4} + C_{NL5}S^3)C_\mu} \quad (11)$$

$$C_3 = \frac{C_{NL3}}{(C_{NL4} + C_{NL5}S^3)C_\mu} \quad (12)$$

where the coefficients  $C_{NL1}$ - $C_{NL5}$  are summarized in Table I.

**Table I. Model coefficients**

$\sigma_k$	$\sigma_\epsilon$	$C_{\epsilon 1}$	$C_{\epsilon 2}$	$C_{NL1}$	$C_{NL2}$	$C_{NL3}$	$C_{NL4}$	$C_{NL5}$
1.0	1.22	1.44	1.92	0.8	11	4.5	1000	1.0

## 2.2. Wall Treatment

The quadratic model has been implemented using a hybrid scalable wall function approach with two-layer treatment of turbulent quantities. Wall functions bridge the viscosity-dominated near-wall region with that

of the fully turbulent bulk flow. Such methods reduce the computational burden of a simulation as the viscous sublayer near the wall is modeled with a single cell as opposed to resolved completely with finely layered cells. The near wall formulation follows the methodology outlined by Craft et al. [12] and Albets-Chico et al. [13], whereby the  $k$ -equation is solved throughout the entire flow domain and the  $\varepsilon$ -equation is solved only up to the wall-attached elements. Inside the wall layer,  $\varepsilon$  is prescribed by using the law of the wall. For a detailed discussion of the wall function formulation, the interested reader is referred to the Hydra-TH Theory Manual [14].

### 3. MODEL IMPLEMENTATION IN HYDRA-TH

At the onset of this project, the Re-normalization Group (RNG) variant of the  $k$ - $\varepsilon$  model, developed by Yakhot et al. [15], had been already implemented in Hydra-TH. Incorporation of the standard and quadratic  $k$ - $\varepsilon$  models required a restructuring of the class architecture and inheritance scheme. This was accomplished through the creation of a base  $k$ - $\varepsilon$  class from which the model-specific variations (i.e. RNG, standard, and quadratic) would derive. This minimized the coding efforts since functions intrinsic to all models, such as solvers and wall treatment, could be located in the base class. The model-specific formulations, including source terms and Reynolds stresses, were subsequently implemented in these derived classes. This framework will serve to streamline future coding endeavors such as the implementation of the Realizable  $k$ - $\varepsilon$  model by Shih et al. [16].

One challenge with the implementation of the quadratic  $k$ - $\varepsilon$  model is the treatment of the quadratic stress terms in the momentum equation. The best practice is to run Hydra-TH simulations fully-implicitly to leverage the Picard iteration scheme in order to facilitate larger time-steps and ensure stability. Due to the complex formulation of the quadratic terms (Eq. 8), however, an implicit treatment was not practical. The quadratic terms have therefore been treated explicitly in the momentum equation.

### 4. COMPUTATIONAL PROCEDURE

Hydra-TH is an unstructured, finite volume, CFD software that utilizes edge-based algorithms for computation. A Lax-Friedrichs flux approximation is utilized, whereby the flux at a dual-edge is calculated by reconstructing the field on both sides of the dual-edge, as depicted in Fig. 1.

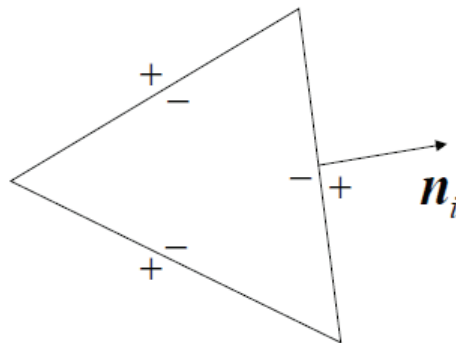


**Figure 1. Reconstructed values for numerical flux calculation (taken from Hydra-TH Theory Manual [14])**

The reconstruction of the field at the dual-edge is calculated using the following expression:

$$u_i^- = \bar{u} + \phi \nabla_c \bar{u} \cdot \delta \mathbf{r}_i \quad (13)$$

Here,  $\bar{u}$  is the cell-centered value;  $\nabla_c \bar{u}$  is a cell-centered gradient that is obtained by performing a weighted least-squares gradient approximation;  $\delta r$  is the distance from the cell-center to the dual-edge; and  $\varphi$  is the gradient limiting procedure, which follows the methodology developed by Barth and Jespersen [17].

Gresho's second-order "P2" projection method [18][19] is used as the pressure-velocity coupling scheme. This approach applies a Helmholtz decomposition to decouple the pressure and velocity into its solenoidal and irrotational components. The irrotational velocity field is calculated and used as a predictor step to solve a pressure Poisson equation to update the pressure and velocity. A non-linear Picard iterative scheme has recently been implemented in order to extend the projection algorithm to a fully-implicit treatment [20].

## 5. MODEL ASSESSMENT

The quadratic  $k-\varepsilon$  model has been applied to triangular and square fuel rod arrays in order to assess its implementation and readiness for reactor simulations. A comparison with the standard  $k-\varepsilon$  model has been performed in order to highlight the importance of capturing the secondary flows generated by anisotropy. In the results that follow, all test cases were performed on a series of refined meshes in order to verify that grid convergence had been achieved.

### 5.1. Triangular Rod Array

A series of velocity and wall shear stress measurements for several Reynolds numbers were performed by Mantlik et al. [21] on a bare triangular rod array. The experiments were performed in a wind tunnel, using nineteen 120 mm outer diameter (OD) rods of 6 m length, with a pitch-to-diameter ratio of 1.17. Measurements were recorded at a distance of 5.6 m from the inlet to ensure that fully-developed flow had been achieved. Pitot and Preston tubes of 0.8 mm (OD) were used to measure the velocity and wall shear stress profiles. The Reynolds number considered in these simulations is 181,200.

Due to the inherent symmetry of the problem, it is sufficient to describe a smaller domain with the prescription of appropriate symmetry boundary conditions (Fig. 2). The domain comprises six elementary flow cells. The rationale for this domain selection originates from leveraging the current implementation of the symmetry boundary conditions in Hydra-TH, which are required to be specified at a surface where its normal directly coincides with a coordinate direction. In the presented results, the elementary flow cell shaded in gray in Fig. 2 is examined.

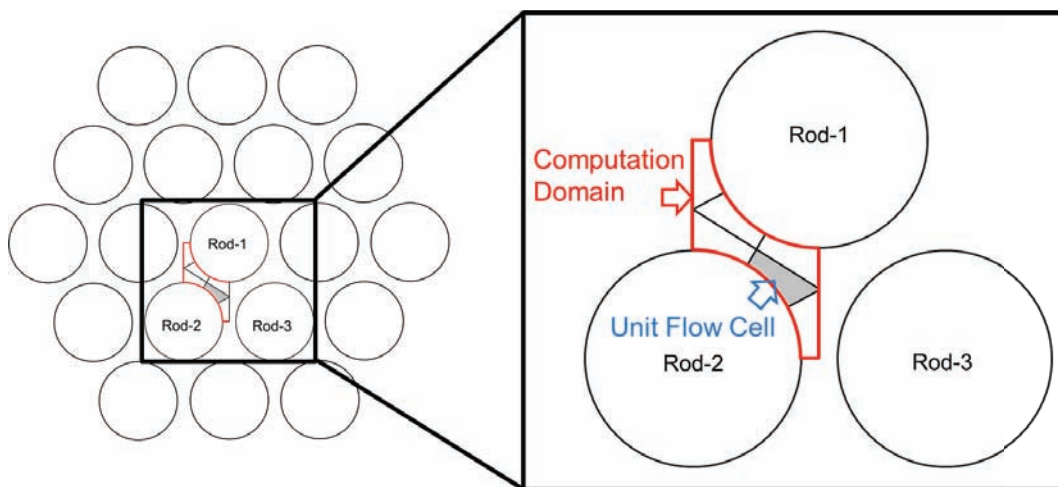


Figure 2. 19-rod bundle experimental configuration [21] (left) and adopted computational domain (right)

The radial velocity profile predictions for the quadratic model are presented in Fig. 3 along with the experimental results. As can be seen, the quadratic model matches the velocity profiles at the angular locations of  $\Phi=15^\circ$  and  $30^\circ$ . For the  $\Phi=0^\circ$  case, the model accurately predicts the velocity in the near wall region, but steadily drifts away from the experimental results as the normal distance to the wall is increased. The quadratic model is also able to match the shape of the wall shear stress distribution measurements, but with a slight underprediction in the  $\Phi=0-12^\circ$  region.

The results of standard  $k-\varepsilon$  model applied to the triangular rod array are also displayed in Fig. 3. Accurate predictions are achieved for the velocity profile at  $\Phi=15^\circ$ ; however, the standard model underpredicts the velocity profile in the narrow region ( $\Phi=0^\circ$ ) and overpredicts it at the  $\Phi=30^\circ$  location. Further, the standard model yields predictions for the wall shear stress that monotonically increase from  $\Phi=0-30^\circ$  and consequently do not coincide with the experimental values. Such behavior is a common observation and known limitation of the standard  $k-\varepsilon$  model that is attributed to the lack of secondary flow prediction, which acts to redistribute the turbulence levels and velocities inside the channel.

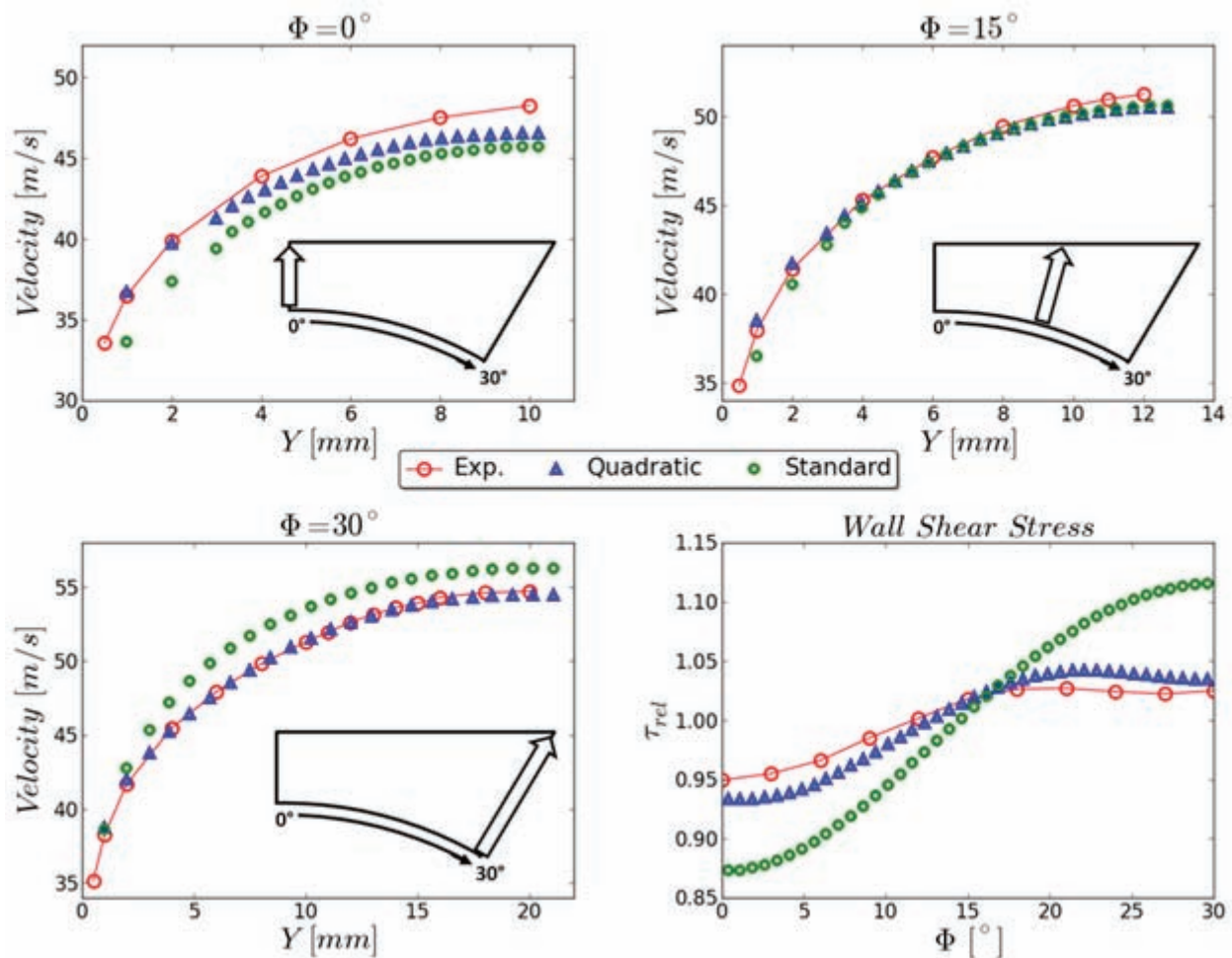
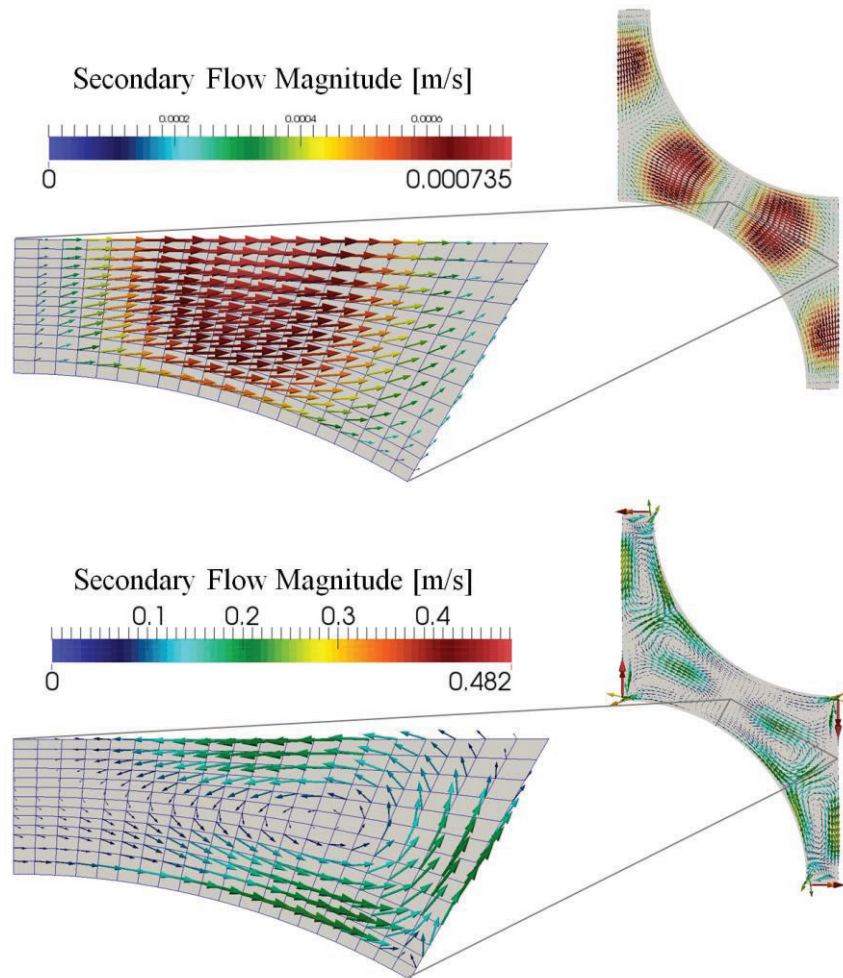


Figure 3. Velocity and wall shear stress distributions (experiment from Mantlik et al. [21])

Fig. 4 illustrates the secondary flows at the plane of measurement for both the quadratic and standard models. A vortex that spans the entire elementary flow cell is observed for the quadratic model, whereas the standard model predicts negligible secondary motion that is simply spurious velocities produced from

the linear eddy viscosity model. Further, the quadratic model predicts magnitudes on the order of 0.1% (in accordance with the experimental measurements of Vonka [5]). These observations confirm that the quadratic model is able to capture the anisotropy driven secondary flow profile, which allows it to resolve the turbulence redistribution, leading to the more uniform axial velocity and wall shear stress profiles depicted in Fig. 3.



**Figure 4. Secondary flow profiles for standard (top) and quadratic (bottom)  $k-\epsilon$  models for a triangular rod array (experiment from Mantlik et al. [21])**

Finer inspection of the secondary flows predicted by the quadratic model sheds insight into why the velocity profile and wall shear stress distributions were underpredicted in the  $\Phi=0-12^\circ$  region. The secondary flow profile is noticeably weaker in this area, which suggests an insufficient level of turbulence to redistribute, leading to a more uniform flow profile. This is an artifact of the code framework that will have to be examined further.

## 5.2. Square Rod Array

A similar analysis of velocity and wall shear stress measurements for varying Reynolds numbers was performed by Hooper and Wood [22] for a bare square rod array. The experimental setup consisted of six rods of 7 cm radius and 9.14 m length, with a pitch-to-diameter ratio of 1.107. Pitot and Preston tubes of

1.6 mm OD were used to measure the velocity and wall shear stress profiles just before the outlet. The Reynolds number considered in these simulations is 207,600. The computational domain consists of two elementary flow cells, as depicted in Fig. 5.

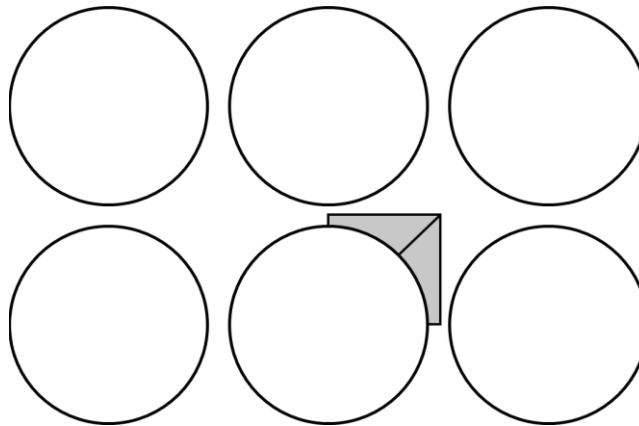


Figure 5. Square rod array configuration of Hooper and Wood [22]

Simulation results for the square rod array are shown in Fig. 6, where the standard and quadratic models are both plotted for comparison. The quadratic model matches the radial velocity profile at  $\Phi=45^\circ$ , but drastically underpredicts the velocity profile at the  $\Phi=0^\circ$  location. The wall shear stress prediction is quite unexpected, as it initially increases with the angle  $\Phi$ , levels off around  $\Phi=30-35^\circ$ , and dips down considerably afterwards. The standard model underpredicts the velocity in the near-wall region—to an even greater extent than the quadratic model—and overpredicts it at the  $\Phi=45^\circ$  location; likewise, the predicted wall shear stress profile is monotonically increasing from  $\Phi=0-45^\circ$  and therefore does not reproduce the experimental trends.

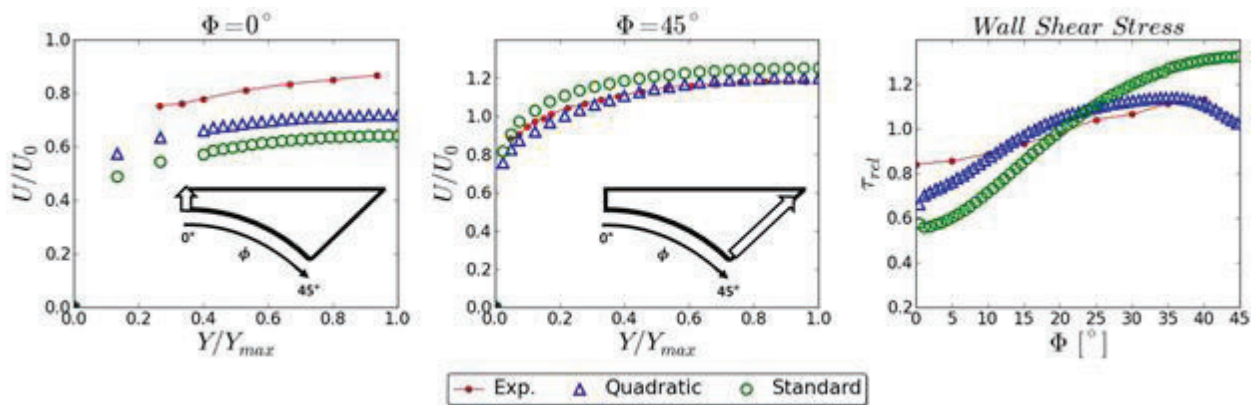
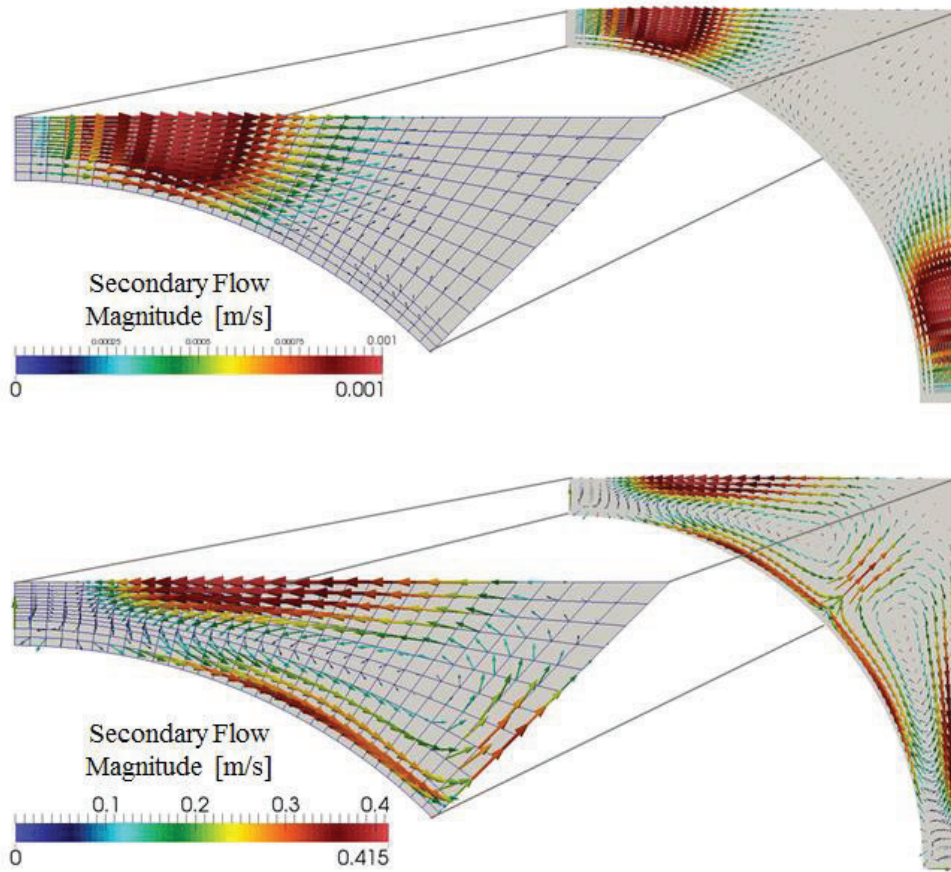


Figure 6. Velocity distributions along the diagonal and wall shear stress profile for Hooper and Wood [22]

The secondary flow profiles for both the quadratic and standard model are shown in Fig. 7. As observed with the triangular array, the quadratic model predicts a spiraling vortex with a magnitude that is approximately 0.1% that of axial velocity profile, while the standard model predicts negligible secondary flows. It is noticeable that the secondary flow profile breaks down near the corners of the simulation for the

quadratic model. This behavior is related to the imperfect implementation of symmetric boundary conditions, as evidenced by the comparison between boundary and internal unit cell results in Fig. 4.



**Figure 7. Secondary flow profiles for standard (top) and quadratic (bottom)  $k-\epsilon$  models (experiment from Hooper and Wood et al. [22])**

### 5.3. Grid Refinement Study

A grid refinement study was performed for both the triangular and square rod array test cases in order to examine the convergence of the simulation. Three prism layers, each with a thickness of 1 mm, were used for both test cases. This corresponded to a  $y^+$  in the range of 50-60 for the triangular rod array and 40-60 for the square rod array. A refinement ratio of two was used for both the radial and azimuthal directions, while the axial refinement was held constant. The elementary meshes used to construct the full geometry are displayed in Fig. 8. Note that the value used to define radial refinement does not include the three wall layer elements.

The grid convergence of both the standard and quadratic  $k-\epsilon$  models for the triangular and square array are displayed in Figs. 9 and 10, respectively. The standard model behaves near identically for all three refinements for both cases, which is a prime indicator that grid convergence is achieved. Conversely, the quadratic model did not achieve proper convergence for the coarsest mesh in both configurations. The two finer meshes did achieve convergence and their values are almost superimposed, which implies that good convergence is obtained for the two fine grids.

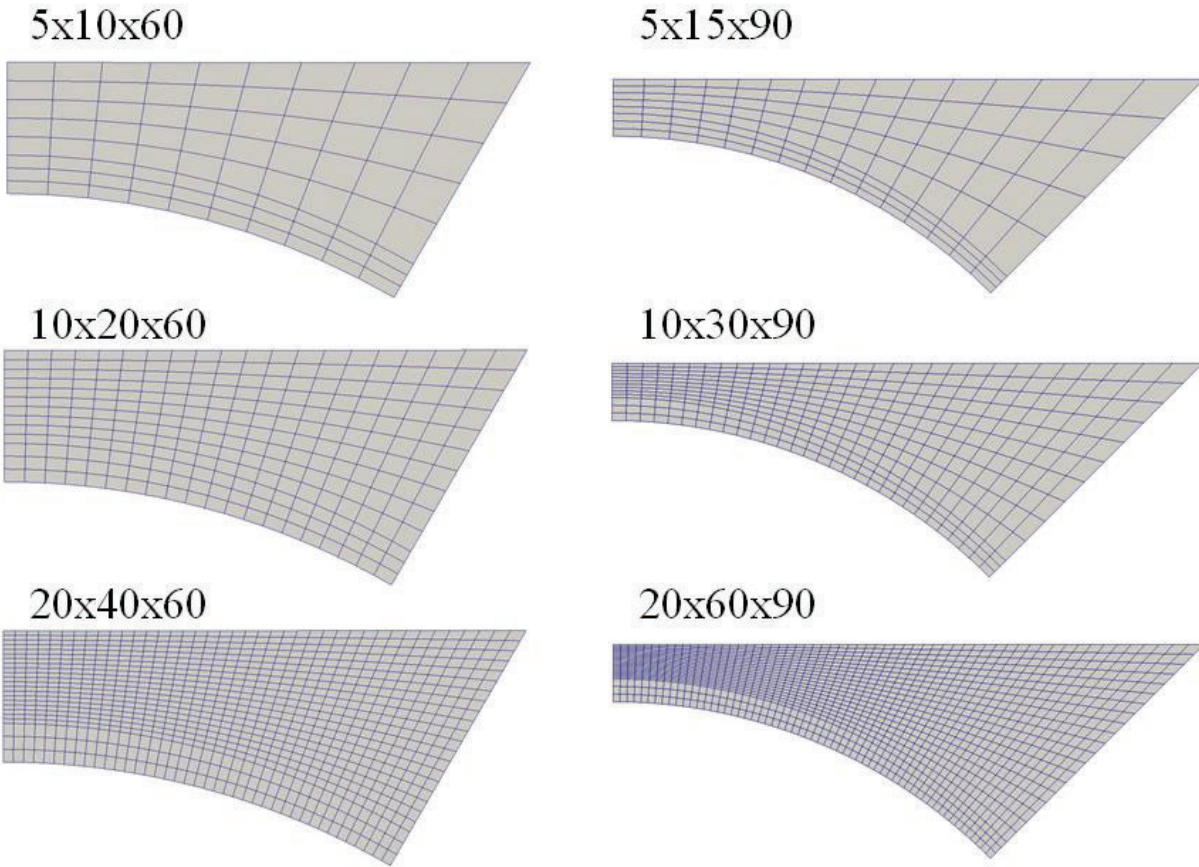


Figure 8. Grid refinement for the triangular array (left) and square array (right)

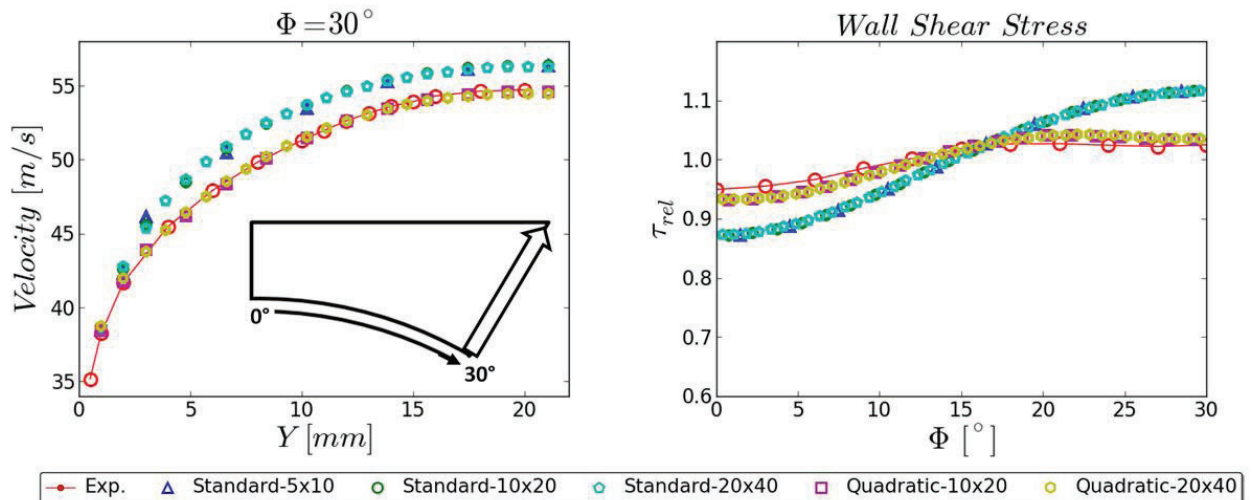


Figure 9. Grid convergence for simulations of triangular rod array experiment by Mantlik et al. [21]

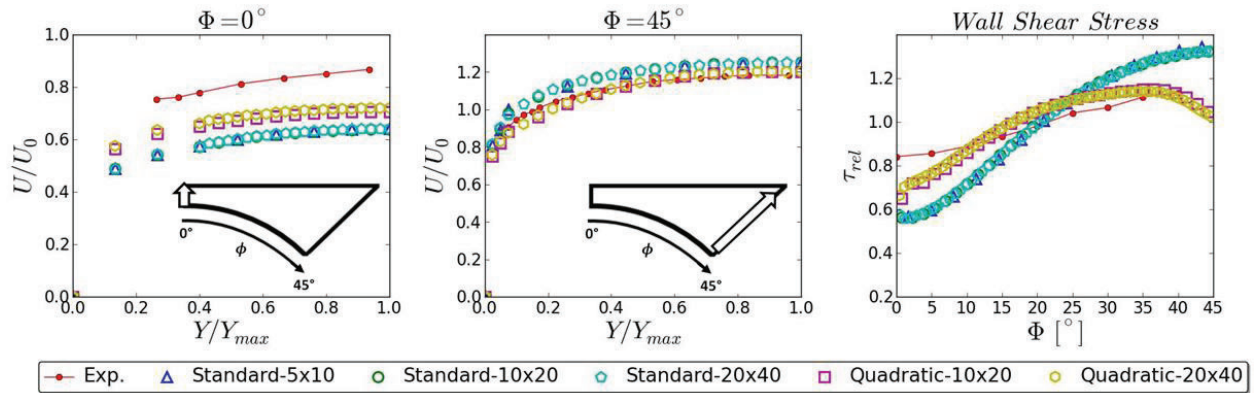


Figure 10. Grid convergence for simulations of square rod array experiment of Hooper and Wood [22]

A Richardson extrapolation of the maximum velocity in the computational domain could only be performed for the standard model, as the coarsest mesh for the quadratic model did not converge. The order of convergence and error on the finest grid for the standard model are listed in Table II. While these values seem nonsensical, the spread of the maximum velocity values for the standard and quadratic models is quite small, which demonstrates that the results reported for the finest mesh reflect a grid-converged solution.

As a final note, the inability of the coarsest mesh to converge for the quadratic model applied to the triangular and square fuel rod arrays is due to the fact that the meshes were simply too coarse. That is, the number of cells is insufficient to resolve the secondary flows, which prevented the simulation from reaching a solution, and is not attributed to a specific shortcoming of neither the solver nor the model implementation.

Table II. Richardson extrapolation results

	Triangular Rod Array [21]		Square Rod Array [22]	
	Quadratic	Standard	Quadratic	Standard
<b>Finest Mesh: <math>V_{\max}</math> [m/s]</b>	54.485	56.285	31.832	31.136
<b>Refined Mesh: <math>V_{\max}</math> [m/s]</b>	54.603	56.381	31.839	31.135
<b>Coarsest Mesh: <math>V_{\max}</math> [m/s]</b>	N/A	56.299	N/A	33.030
<b>Max Spread [m/s]</b>	0.118	0.096	0.0066	0.1057
<b>Order of Accuracy</b>	N/A	0.227	N/A	6.571
<b>Error on Finest Grid [m/s]</b>	N/A	0.562	N/A	$1.17 \times 10^{-5}$

#### 5.4. Best Practices and Guidelines

A comprehensive sensitivity study for the quadratic model applied to the triangular fuel rod array experiments by Mantlik et al. [21] was performed by Magolan [23] in order to derive best practices and guidelines for its application to nuclear fuel related problems. The impact that the number of wall layer elements, symmetry boundary conditions, axial refinement, and time-step pose on the convergence were each examined in the work. The resulting conclusions are summarized herein.

### 5.4.1. Wall layer treatment

The use of a single wall layer element was discovered to be insufficient to ensure proper convergence of the quadratic model. Adopting two or three wall layer elements proves robust on all tested configurations for varying thicknesses.

The lack of grid convergence when using one wall layer element is attributable to the hybrid two-layer wall-function approach that is used in the Hydra-TH to model the near-wall region. Since the  $k$ -equation is solved up to the wall, the resulting solution is therefore particularly sensitive to the elements in the near-wall region, and the resulting grid refinement near the wall has a significant impact on the distribution. Additional wall layers are therefore critical.

### 5.4.2. Computational domain and coordinate symmetry

Simulation of a single elementary cell versus the full computational domain that comprises six elementary cells (Fig. 2) was examined to assess the impact of the boundary conditions on the resulting solution. If capturing the dominant flow features such as the axial velocity profile is the objective, then the use of a single elementary flow cell should be sufficient as it would be computationally cheaper and promote a faster run-time. However, if resolving the impact of secondary flows is critical for adequate simulation of the problem, then great care should be taken to construct a geometry that respects the coordinate symmetry. An example of this includes resolving the wall shear stress distribution, which is used to predict the heat transfer coefficient.

### 5.4.3. Axial refinement

The use of very large aspect ratios does not demonstrate an appreciable impact on the effect and generation of turbulence driven secondary flows that arise from the channel geometry. However, this assertion may not be valid when the secondary flows themselves are greatly enhanced by turbulence, such as the case with mixing vanes on fuel assembly grids. In these instances, greater refinement of the mesh downstream is advisable.

### 5.4.4. Maximum CFL number and convergence

Due to the explicit treatment of the quadratic stress terms in the momentum equation, the Courant-Friedrichs-Lewy (CFL) number should be limited to ensure proper convergence. It was discovered that a maximum CFL number in the range of 0.1 – 0.25 is sufficient to achieve convergence. It is highly advised to begin the simulation with an even smaller CFL number (e.g. 0.001) and employ a time-step growth factor to increase the CFL number to its maximum specified limit.

## 6. CONCLUSIONS

The NLEVM developed by Baglietto and Ninokata [10] has been implemented into Hydra-TH. This model applies a quadratic formulation of the stress-strain relationship that captures the anisotropy of the normal stresses and is able to resolve the complex secondary vortices that arise in nuclear reactor fuel assemblies. Restructuring of the code framework and  $k$ - $\varepsilon$  class inheritance schemes was required in order to accommodate the incorporation of both the standard and quadratic  $k$ - $\varepsilon$  model implementations.

Model assessment has been performed through simulation of the triangular and square rod array experiments of Mantlik [21] and Hooper and Wood [22]. The quadratic formulation has demonstrated the ability to resolve the complex secondary flow structures as well as predict velocity and wall shear stress

distributions. Comparison of the quadratic model with that of the standard model allows for a greater appreciation for the utility of the model, and clearly asserts the need for resolving flow anisotropy.

The results of this study show great promise for the quadratic  $k$ - $\varepsilon$  model's application to nuclear reactor systems. The quadratic model complements the already validated LES implementation, which together provide a balanced modeling and simulation capability for the Hydra-TH toolkit. Future work will seek to extend the evaluation of the model to realistic fuel assembly configurations, including mixing vane spacers, in order to derive guidelines and best practices for its application to complex flow geometries. The model also promises greater generality and its application will be evaluated for simulation of flow inside the reactor vessel, during both operational and transient conditions.

## NOMENCLATURE

$k$	Turbulent kinetic energy
$P_k$	Production rate of turbulent kinetic energy
$S_{ij}$	Mean strain rate tensor
$y$	Normal distance from wall
$y^+$	Non-dimensionalized distance from wall
$u_i$	Velocity components ( $i = 1,2,3$ )
$\overline{u'_i u'_j}$	Reynolds stress tensor

## Greek Letters

$\delta_{ij}$	Kronecker delta
$\varepsilon$	Turbulent dissipation rate
$\rho$	Density
$\Omega$	Mean rotation rate tensor
$\mu$	Molecular viscosity
$\mu_t$	Turbulent viscosity

## ACKNOWLEDGMENTS

The authors would like to thank the CASL project and the Rickover Fellowship Program for supporting this work.

## REFERENCES

1. C. Trupp and R.S. Azad, "The structure of turbulent flow in triangular array rod bundles," *Nucl. Eng. Des.*, **32**(1), pp. 47-84 (1975).
2. P. Carajilescov and N.E. Todreas, "Experimental and Analytical Study of Axial Turbulent Flows in an Interior Subchannel of a Bare Rod Bundle," *J. Heat Transfer*, **98**(2), (1975).
3. K. Rehme, "Experimental observations of turbulent flow through subchannels of rod bundles," *Experimental Thermal and Fluid Science*, **2**(3), pp. 341-349 (1989).
4. J. Nikuradse, "Untersuchung ueber die Geschwindigkeitsverteilung in turbulenten Stroemungen," Diss. Gottingen, VDI-forschungsheft 281 (1926).
5. V. Vonka, "Measurement of secondary flow vortices in a rod bundle," *Nucl. Eng. Des.*, **106**(2), pp. 191-207 (1988).
6. J.L. Lumley, "Toward a turbulent constitutive relation," *J. Fluid Mechanics*, **41**(2), pp. 413-434 (1970).
7. S.B. Pope, "A more general effective-viscosity hypothesis," *J. Fluid Mechanics*, **72**(2), pp. 331-340 (1975).

8. E. Baglietto, "Anisotropic Turbulence Modeling for Accurate Rod Bundle Simulations," *Proceedings of 14<sup>th</sup> International Conference on Nuclear Engineering (ICONE14)*, Miami, Florida, July 17-20, (2006).
9. E. Baglietto and H. Ninokata, "A turbulence model study for simulating flow inside tight lattice rod bundles," *Nucl. Eng. Des.*, **235**(7), pp. 773-784 (2005).
10. E. Baglietto and H. Ninokata, "Anisotropic Eddy Viscosity Modeling for Application to Industrial Engineering Internal Flows," *Int. J. Transport Phenomena*, **8**(2), pp. 85-101 (2006).
11. B.E. Launder and D.B. Spalding, "The numerical computation of turbulent flows," *Comp. Meth. in Appl. Mech. And Eng.*, **3**(2), pp. 269-289 (1974).
12. T.J. Craft, A.V. Gerasimov, H. Lacovides, B.E. Launder, "Progress in the generalization of wall-function treatments," *Int. J. Heat and Fluid Flow*, **23**(2), pp. 148-160 (2002).
13. X. Albets-Chico, C.D. Perez-Segarra, A. Olivia, J. Bredberg, "Analysis of wall-function approaches using two-equation turbulence models," *Int. J. Heat and Mass Transfer*, **51**(19-20), pp. 4940-4957 (2008).
14. M.A. Christon, J. Bakosi, M.M. Francois, and R. Nourgaliev, "Hydra-TH Theory Manual," Tech. Rep. LA-UR 11-05387, Los Alamos National Laboratory, revised November 2013.
15. V. Yakhot, S. Thangam, T.B. Gatski, S.A. Orszag, and C.G. Speziale, "Development of Turbulence Models for Shear Flows by a Double Expansion Technique," *Physics of Fluids*, **4**(7), pp. 1510-1520 (1992).
16. T.-H. Shih, J. Zhu, and J.L. Lumley, "A Realizable Reynolds Stress Algebraic Equation Model," NASA TM (1993).
17. T.J. Barth and D.C. Jespersen, "The design and application of upwind schemes on unstructured meshes," *AIAA 27<sup>th</sup> Aerospace Sciences Meeting*, Reno, Nevada, January 9-12, AIAA-89-0366 (1989).
18. P.M. Gresho, "On the theory of semi-implicit projection methods for viscous incompressible flow and its implementation via a finite element method that also introduces a nearly consistent mass matrix. part 1: Theory," *Int. J. Numerical Methods in Fluids*, **11**(5), pp. 587-620 (1990).
19. P.M. Gresho and S.T. Chan, "On the theory of semi-implicit projection methods for viscous incompressible flow and its implementation via a finite element method that also introduces a nearly consistent mass matrix. part 2: Implementation," *Int. J. Numerical Methods in Fluids*, **11**(5), pp. 621-659 (1990).
20. R. Nourgaliev, M. Christon, J. Bakosi, and A. Bui, "Newton-Krylov Based P2 Projection Solver for Fluid Flows," Tech. Rep. INL/EXT-13-28278, Idaho National Laboratory, June 2013.
21. F. Mantlik, J. Heina, and J. Chervenka, "Results of local measurements of hydraulic characteristics in triangular pin bundle," UJV=3778-R, Rzez, Czech Republic (1976).
22. J.D. Hooper and D.H. Wood, "Fully developed rod bundle flow over a large range of Reynolds number," *Nucl. Eng. Des.*, **83**(1), pp. 31-46 (1984).
23. B. Magolan, "Implementation of a Non-Linear Eddy Viscosity Turbulence Model into Hydra-TH for Fuel Related Applications," M.S. Thesis, MIT, June 2015.